Pol. J. Environ. Stud. Vol. 33, No. X (2024), 1-9
DOI: *10.15244/pjoes/183707* ONLINE PUBLICATION DATE:

Original Research

Studies on Photophysical and Biological Activity of Newly Synthesized of 4-Methylpiperidin-4-ol Substituted Pyrazole Derivatives

Ghaferah H. Al-Hazmi[1], Vidyagayatri Marrakkur[2], Lohit Naik[3], Moamen S. Refat[4*]

[1]Department of Chemistry, College of Science, Princess Nourah bint Abdulrahman University, P.O. Box 84428, Riyadh 11671, Saudi Arabia
[2]Department of Chemistry, NMKRV College for Women, Bengaluru-560006, India
[3]Department of Physics and Electronics, CHRIST (Deemed to be University), Bengaluru-560029, India
[4]Department of Chemistry, College of Science, Taif University, P.O. Box 11099, Taif 21944, Saudi Arabia

Received: 5 November 2023
Accepted: 5 February 2024

Abstract

The in vitro antifungal, antibacterial, and antioxidant activities of a substituted pyrazole derivative (FHM) have been evaluated in the current work. The addition of 4-methylpiperidin-4-ol, which increases the molecule's lipid solubility and speeds up absorption by increasing its rate of absorption, gives the molecule strong in vitro antifungal and antibacterial properties. Additionally, it is clear from the findings of structure-activity relationship (SAR) investigations. Additionally, the *ab-intio* technique was used to theoretically evaluate the photophysical characteristics of produced substances. Using the DFT-B3LYP-6-31G(d) basis set, the ground state optimization and HOMO-LUMO energy levels are computed. Global chemical reactivity and descriptive characteristics are evaluated using theoretically estimated HOMO-LUMO values, and the results demonstrate that the synthesized molecule possesses a high electrophilicity and electronegative index. Overall findings indicate that substituting a 4-methylpiperidin-4-ol substituted pyrazole derivative shows good photophysical and *in vitro* biological applications.

Keywords: Pyrazoles, *in-vitro* and *in-silico* biological activity, HOMO-LUMO, GCRD parameters.

Introduction

In recent years, the field of organic chemistry has witnessed remarkable advancements in the synthesis of novel compounds with diverse applications, ranging from pharmaceuticals to optoelectronic materials. Pyrazole derivatives have garnered significant attention due to their versatile nature and potential for biological and optoelectronic applications.

Pyrazoles refer to a group of compounds with a core structure of 1H-pyrazol-3-ol and pyrazolin-5-one. These compounds have been extensively studied due to their various properties and applications [1]. The promising analgesic and antipyretic effects observed in pyrazolone analogs prompted researchers to seek out other derivatives with similar properties but even

*e-mail: msrefat@yahoo.com

more potent therapeutic actions. As of today, numerous drugs containing the pyrazolone nucleus have received approval from the Food and Drug Administration. For example, edaravone has been employed as a free radical scavenger in treating amyotrophic lateral sclerosis [2]. Aminophenazone is utilized in breath tests to measure cytochrome P-450 metabolic activity in liver function assessments because of its antipyretic and anti-inflammatory effects [3]. Eltrombopag is effective in treating people with idiopathic chronic immune thrombocytopenia who have low blood platelet counts [4]. It is recommended to take dichloralphenazone to treat tension and vascular headaches [5]. Metamizole has been effectively employed for perioperative pain, cancer-related pain, acute injuries, and various other types of pain, being considered one of the most potent antipyretic agents [6]. Furthermore, several investigational small molecules containing the pyrazolone structure are under consideration as potential drug candidates, including sulfamazone [7], propyphenazone [8], and nifenazone [9]. In the realm of biology, pyrazoles exhibit a plethora of biological activities and have been extensively studied for their potential therapeutic applications. These activities include antibacterial, anticancer, anti-inflammatory, antifungal, and antimalarial properties. In addition, pyrazole-cored organic frameworks were also known for their tangible fluorescence properties, but they were less explored [10].

The goal of the present work is to synthesize a 4-methylpiperidin-4-ol substituted pyrazole derivative (FHM) using low toxic regents. Further, estimate their biological and photophysical properties using experimental and theoretical techniques.

Materials and Methods

Commercial samples of high purity were utilized as received for the reagents (Fischer, Merck, and Sigma Aldrich). An RB flask that had been oven dried was used for the reactions. Alumina silica gel 60F254 (Fischer) underwent TLC after being detected by iodine vapors and UV light (254 nm). Uncorrected open capillaries on a Buchi apparatus were used to determine the melting points. Using KBr pellets, the IR spectra were captured on a Nicolet-Impact-410 FT-IR spectrometer. Using TMS as an internal standard and a Bruker AC-400F 400 MHz spectrometer, the resonance frequencies for the ^{1}H-NMR and 13C-NMR spectra were 400 MHz and 100 MHz, respectively. Agilent 1200 series equipment was used to conduct LCMS analyses. The Heraus CHN fast analyzer was used to do elemental analysis. All the compounds produced C, H, and N analyses that were within 0.4% of the predicted values.

Synthesis of a 4-Methylpiperidin-4-ol Substituted Pyrazole Derivative (FHM)

Compound (3) was synthesized by combining 1 mmol of β-diketoester with 4-fluorophenyl hydrazine in a solution containing 100 ml of ethanol and 10 ml of acetic acid. The mixture was refluxed overnight, and after removing ethanol by concentration, the reaction mixture was neutralized with Na_2CO_3. The resulting solid was then filtered, dried, and further purified through recrystallization using ethanol. Subsequently, pyrazole carboxylic acid ethyl ester (3), 1 mmol of the compound, was dissolved in 50 ml of tetrahydrofuran

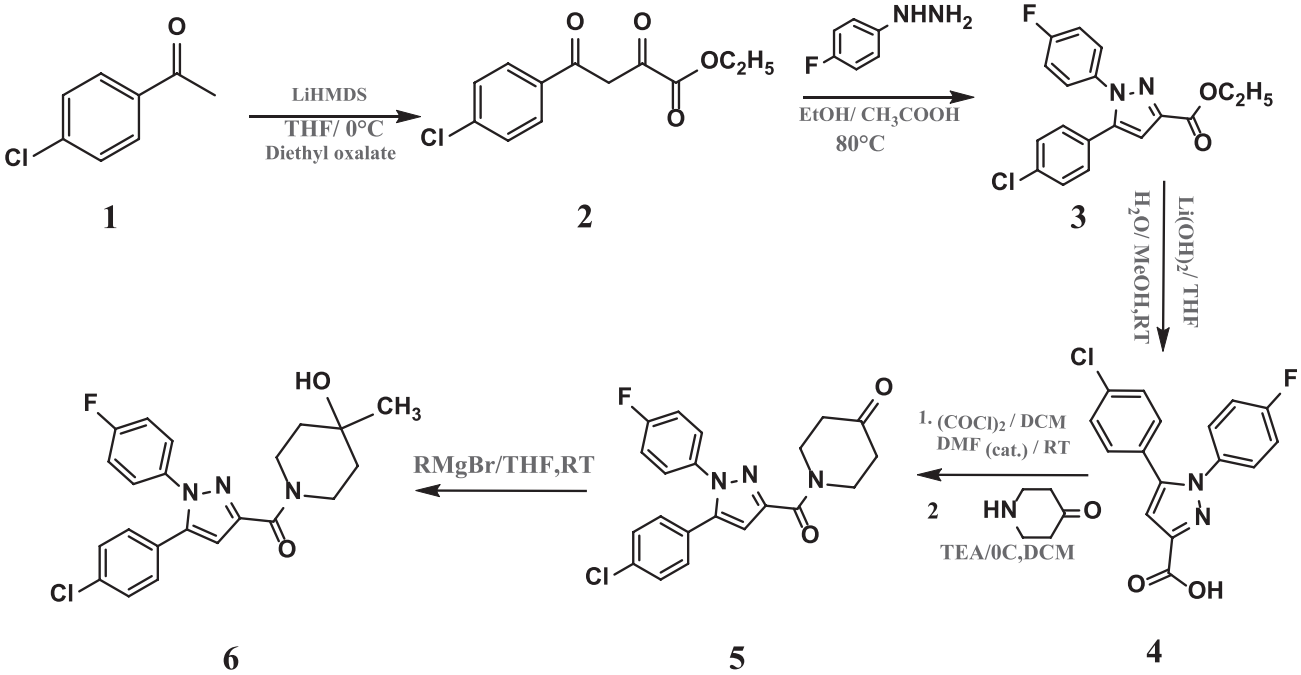

Scheme 1. Synthesis of a 4-methylpiperidin-4-ol substituted pyrazole derivative (FHM).

(THF). Then, 15 ml of methanol, 20 ml of water, and 1.2 mmol of lithium hydroxide were added, and the mixture was stirred overnight. After the reaction, the solvent was concentrated to remove volatile components. The resulting residue was dissolved in a solution comprising 50 ml of water and 100 ml of ethyl acetate. The solution was acidified to a pH of approximately 5 using 1N HCl and extracted with 100 ml of ethyl acetate twice. The combined organic layer was washed with 50 ml of water and a brine solution of 20 ml, dried using Na_2SO_4, and evaporated to dryness, yielding compound (4). For the preparation of compound (5), 1 mmol of compound (4) was dissolved in 20 ml of dichloromethane (DCM). Then, 1.5 mmol of oxalyl chloride was added at 0°C, and after 5 minutes, a catalytic amount of dimethylformamide (DMF) in the form of 3 drops was introduced. The mixture was stirred at room temperature. Once the reaction was complete, excess oxalyl chloride was removed under nitrogen, resulting in the formation of pure acid chloride. This acid chloride was then dissolved in fresh DCM (25 ml). At 0ºC, 2 mmol of triethylamine was added to the solution, followed by the addition of 1.1 mmol of 4-piperidone, also at 0ºC. After the reaction was finished, the mixture was diluted with 50 ml of water and extracted with DCM twice (2×100 ml). The combined organic layer was washed with 50 ml of water and a brine solution consisting of 20 ml, dried with Na_2SO_4, and evaporated to dryness. The crude products were further purified by washing with diethyl ether. Finally, to prepare compound (6), 1 mmol of compound (5) was taken in THF (20 ml), and 1.5 mmol of Grignard reagent was added at 0ºC. After the reaction was complete, the mixture was allowed to reach room temperature. The reaction's progress was monitored by TLC. The reaction mixture was quenched with saturated ammonium chloride and extracted with ethyl acetate twice (2×100 ml). The combined organic layer was washed with 50 ml of water and a brine solution of 20 ml, dried over Na_2SO_4, and evaporated to dryness. The crude products were purified by column chromatography using 230-400 silica gel.

Structural Characterization of the (5-(4-Chlorophenyl)-1-(4-Fluorophenyl)-1H-Pyrazol-3-yl) (4-Hydroxy-4-Methylpiperidin-1-yl) Methanone (FHM)

White solid, mp 92.8ºC; % yield: 67; ^{1}H NMR (300MHz, $CDCl_3$): δ = 7.32(m, 3H, ArH), 7.28(m, 1H, ArH), 7.24(m, 2H, ArH), 7.04(m, 2H, ArH), 6.87(s, 1H, pyrazole CH), 4.40(m, 2H, -CH_2), 3.69(m, 1H, -CH), 3.38(m, 1H, -CH), 1.72(m, 4H, -CH_2-CH_2), 1.26(s, 3H, -CH_3); MS calcd. for $C_{22}H_{21}ClFN_3O_2$: 413.7, Found: 414.2(M+); IR (ν cm^{-1}): 3351(O-H), 3111(Ar-H), 1622(C=O); Elem. Anal. cald (found): C: 63.84(63.80), H: 5.11(5.09), N: 10.25(10.12).

In Vitro Antifungal Studies

Newly synthesized pyrazoles were evaluated for their antifungal effectiveness against two fungal strains, A. niger and C. albicans, using the serial plate dilution method in a DMSO solution [11, 12]. A Sabouraud agar medium was prepared by dissolving 1g of peptone, 4 g of D-glucose, and 2 grams of agar in 100 ml of distilled water, adjusting the pH to 5.7. Spore suspensions for the fungal strains were prepared using ordinary saline. To create these suspensions, a loopful of the respective fungal strain was mixed with 3 ml of saline. Twenty milliliters of agar medium were poured into each Petri dish. After decanting the excess suspension, the plates were allowed to dry for one hour at 37ºC in an incubator. These seeded agar plates were then punctured, and each well was appropriately labeled. Subsequently, test chemicals in DMSO, ranging from 10 g/mL to 50 g/mL, were added to different wells. Control plates were also prepared using DMSO as the solvent. All Petri dishes were replicated three times and incubated at 37ºC for three to four days. The antifungal activity was determined by measuring the inhibition zone, and the results were compared to those of Fluconazole, a commonly used antifungal drug.

In Vitro Antibacterial Studies

The antibacterial potential of newly synthesized pyrazoles was investigated against a panel of bacterial strains, including S. aureus, B. subtilis, E. coli, and S. typhi, using the disc diffusion method [11, 12]. Discs with a diameter of 6.25 mm were punched from Whatman No. 1 filter paper. To ensure sterility, batches of 100 discs were placed in screw-capped bottles and subjected to dry heat at 140ºC for one hour. The test compounds were prepared in various concentrations using dimethyl sulfoxide (DMSO). Each bottle contained 100 discs, with each disc impregnated with 1 mL of the chemical at a 100-fold concentration. Discs of each concentration were placed in separate wells of nutrient agar medium, which had been previously inoculated with the target bacteria. Incubation was carried out at 37ºC for a period of twenty-four hours. Controls included discs with only the solvent and discs without any chemicals, allowing for the assessment of growth inhibition. The zones of inhibition and minimum inhibitory concentrations (MICs) were carefully recorded. The obtained results were then compared with those of the standard antibiotic, ciprofloxacin.

Results and Discussion

Computational Photophysical Studies

For physicists and chemists, molecular orbitals and associated attributes, such as energy levels, are useful tools. The most reactive sites in electron systems may

be predicted using these orbitals, specifically the border electron density, which also helps to explain different reactions in conjugated systems [13]. The energy gap between the lowest unoccupied molecular orbital (LUMO) and the highest occupied molecular orbital (HOMO), as well as their respective eigenvalues, also sheds light on a molecule's chemical reactivity. Notably, the bioactivity brought on by intramolecular charge transfer (ICT) has recently been demonstrated using the energy gap between the HOMO and LUMO [14, 15].

The freshly synthesized FHM molecules ground state was optimized using the DFT-B3LYP/6-31G (d) basis set in the Gaussian-09W program. Figs. 1-2 display the FHM molecule HOMO-LUMO, energy gap, and optimized molecular geometry. According to the HOMO-LUMO plot, the π–orbital of the HOMO electron cloud is primarily distributed across the molecule, while the unfilled π*–orbital LUMO is in position five (4-chlorophenyl) -1-(4-fluorophenyl) -1H-pyrazole-3-carbaldehyde.

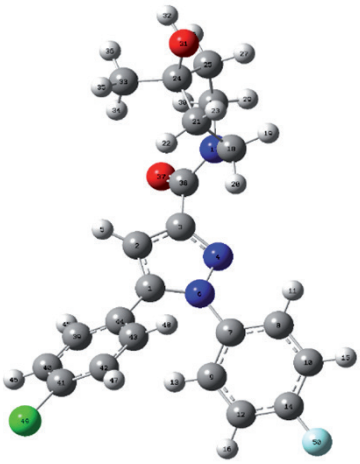

Fig. 1. Optimized molecular geometry with atomic labels of the FHM molecule.

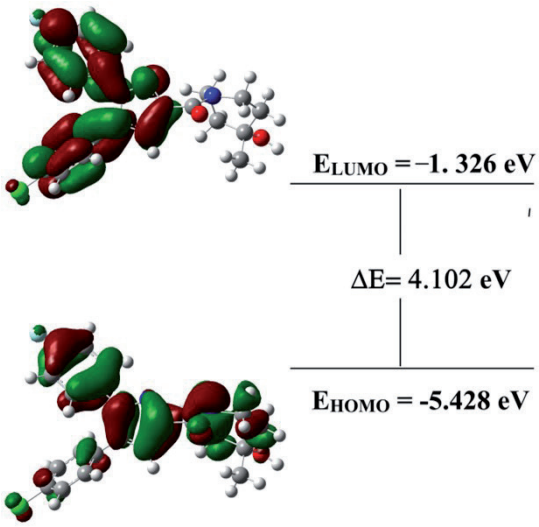

Fig. 2. 3D plots of HOMO-LUMO with energy levels for the FHM molecule.

To gain insight on the chemical reactivity and stability of FHM molecules, global reactivity parameters [16] were calculated using the following Eq. (1) to (5).

$$\eta = \frac{(IP-EA)}{2} \quad (1)$$

$$\chi = \frac{(IP+EA)}{2} \quad (2)$$

$$\mu = -\chi \quad (3)$$

$$S = \frac{1}{2\eta} \quad (4)$$

$$\omega = \frac{\mu^2}{2\eta} \quad (5)$$

Chemical hardness (η = 2.051 eV), electronegativity (χ = 3.377 eV), chemical potential (μ = −3.377 eV), chemical softness (S = 0.244 eV) and electrophilicity index (ω = 2.780 eV) were calculated from E_{HOMO} and E_{LUMO} values [16], where, ionization potential, $IP - E_{HOMO}$ = 5.428 eV and electron affinity, $EA - E_{LUMO}$ = 1.326 eV. While a wider HOMO–LUMO gap relates to stability and hardness, a lesser HOMO–LUMO gap signifies a more reactive soft molecule, which is highly polarizable.

The lowest unoccupied molecular orbit (LUMO), which accepts electrons during molecular interactions, has an energy that is related to the electron affinity ($EA = -E_{LUMO}$), whereas the highest occupied molecular orbit (HOMO), which represents electron donors, has an energy that is related to the ionization potential ($IP = -E_{HOMO}$). A molecule with a large HOMO-LUMO energy gap has high kinetic stability and low chemical reactivity because it is energetically unfavorable to add an electron to the high-lying LUMO in order to remove electrons from the low-lying HOMO. In contrast to compounds with a short HOMO-LUMO energy gap, those with a high HOMO-LUMO energy gap are stable and, as a result, chemically tougher. Accordingly, the compound FHM is hard and more stable (less reactive), according to the GCRD measure. This may be because 1-methylcyclohexan-1-ol was substituted and produced the greatest energy gap by being non-planarly attached to pyrazole. As a result, these substituents make the five-membered ring more reactive.

The deformation of the molecular electron cloud is clearly affected by minor perturbations, demonstrating the underlying resistance that contributes to the hardness seen throughout chemical processes. In contrast to soft molecules, which are bigger and more polarizable, hard molecules are relatively tiny and have reduced polarizability. With softness showing an inverse connection to hardness, hardness plays

a crucial function in communicating the stability and intermolecular reactivity of molecules.

Electrophilicity phenomena are closely tied to the ability of an electrophile to acquire additional electrical charge. The chemical potential (related to electron transfer) and the hardness of a molecule, which signifies its stability, are revealed by the molecule's resistance to the exchange of electrons with its surroundings. An essential quantum chemical descriptor for assessing the reactivity and site selectivity of compounds, particularly in terms of toxicity, is the electrophilicity index [16]. This index, derived from HOMO-LUMO energy values, quantifies the reduction in energy resulting from the maximum electron flow between a donor and an acceptor. A lower value of ω indicates a strong nucleophile, while a higher ω value signifies a potent electrophile. If the electrophilicity scale (ω) is greater than 1.5 eV, an organic molecule is considered a robust electrophile. Electrophiles with values ranging between 0.8 eV and 1.5 eV are regarded as moderate electrophiles, while those with electrophilicity values below 0.8 eV are categorized as weaker electrophiles [17, 18].

Our research findings indicate that the FHM molecules described herein exhibit strong electrophilic characteristics, as evidenced by their elevated ω values. Chemical potential (μ) is used to describe the propensity of electrons to exit a stable system. A complex with a negative chemical potential value is considered stable and does not spontaneously disintegrate into its constituent parts. The FHM molecules, as indicated by their negative chemical potentials, do not undergo such disintegration. The HOMO-LUMO gap, which measures chemical hardness at an energy level of 4.055 eV, suggests that these molecules are less polarizable and demonstrate resistance to the deformation of the electron cloud within the chemical system under moderate disturbances.

Antimicrobial, Antifungal, and Antioxidant Activity

The newly synthesized compound FHM was the subject of antimicrobial investigations, yielding remarkable antibacterial efficacy against *S. aureus*, *B. subtilis*, *S. typhi*, and *E. coli*, as detailed in Table 1. Moreover, the FHM molecule demonstrated strong antifungal activity against *A. niger* and *C. albicans*, with specific data provided in Table 1. The enhanced activity of the compound can be attributed to the presence of biologically active components, including the pyrazole moiety and the 4-methylpiperidin-4-ol ring, which bear similarities to hydrogen in terms of steric requirements at enzyme receptor sites. The inclusion of 4-methylpiperidin-4-ol contributes to an accelerated absorption rate due to its heightened lipid solubility, an attribute that significantly augments the molecules' pharmacological potential [19, 20]. The pronounced lipophilic nature of the bromobenzene group plays a pivotal role in enhancing pharmacological activity. Furthermore, we evaluated the antioxidant properties of FHM molecules and found them to possess exceptional radical scavenging capabilities at the tested concentration of 15 μM, as evidenced in Table 2, in comparison to the standard reference, edaravone. The observed variations in DPPH scavenging capacity can be linked to the impact of diverse substitutions at positions 1, 2, 3, and 5 within the synthesized compounds. These antioxidant activity results align with those seen in previous research findings [21].

Molecular Docking Studies

The molecular structure plays a crucial role in understanding the application and biological activity of a compound. Different functional groups in a molecule can interact with specific biological targets or receptors. Understanding the presence and arrangement of these functional groups helps predict how a molecule will

Table 1. Antimicrobial and antifungal activity of the newly synthesized pyrazoles derivatives.

Compound[b]	*S. aureus*	*B. subtilis*	*S. typhi*	*E. coli*	*A. niger*	*C. albicans*
FHM	25	26	27	27	22	23
Standard[a]	24	23	23	25	25	24
Control[c] DMSO	0	0	0	0	0	0

Note: [a]Standard drug used: Bacteria (Ciprofloxacin), Fungal (Fluconazole) were in 40 μg in 100μL, and R: Resistance
[b]Compounds used: (40 μg in 100μL) and zone of inhibition 26 mm,
[c]Control: DMSO (Dimethyl sulfoxide)

Table 2. DPPH scavenging assay of aryl substituted pyrazoles derivatives.

Compounds Concentration (15 μg/mL)	FHM	Standard (edaravone)
% DPPH scavenging	62.95	73.16

Table 3. Binding energy (Kcal/mol) summary of the FHM compound with the three target proteins

Compounds	DNA Gyrase	Lanosterol 14α demethylase	KEAP1/NRF2
FHM	-4.5	-7.4	-9.3
Ciprofloxacin	-4.6	-	-
Fluconazole	-	-7.8	-
J6Q	-	-	-8.5
Edaravone	-	-	-6.1

interact with biological systems. The three-dimensional arrangement of atoms in a molecule (stereochemistry) is vital. Enantiomers or stereoisomers can exhibit different biological activities due to their distinct interactions with chiral biological receptors. The distribution of electron density within a molecule influences its reactivity. Reactive sites or regions can participate in various biological processes, such as enzyme binding or nucleophilic attacks. The flexibility of a molecule and its ability to adopt different conformations impact its interactions with biological targets. Understanding the potential conformations provides insights into the molecule's behavior in biological environments. Lipophilicity (affinity for lipids) and solubility properties are determined by the molecular structure. These characteristics influence how a molecule is absorbed, distributed, and eliminated in biological systems, affecting its overall bioavailability. The specific arrangement of atoms in a molecule dictates its ability to bind to specific biological targets. Molecular structure influences binding affinity and specificity, crucial factors in determining the biological activity of a compound [22-24].

Molecular docking simulations were performed using AutoDock VINA software integrated into the PyRx 0.8 [25] virtual screening tool for the evaluation of binding affinity. Insilco docking studies were conducted for the assessment of molecular interactions of FHM compounds with antibacterial target, DNA Gyrase (PDB:2XCT), antifungal target, Lanosterol 14 alpha demethylase or CYP51 (PDB:4WMZ), and antioxidant target, KEAP1/NRF2 (PDB:6QME) proteins with a co-crystallized ligand (J6Q). The protein structures were meticulously prepared to ensure optimal configurations for subsequent docking studies. This preparatory process was conducted using the UCSF Chimera Dock Prep module, encompassing the following essential steps: the removal of water molecules and other ligands, the addition of any missing atoms and residues, energy minimization, and the assignment of charges and polar hydrogens. The resulting structures were then converted into the pdbqt format. In parallel, the 2D structures of the ligands were sketched using ChemDraw software, followed by structural optimization through energy minimization employing MMFF94 force field parameters and a conjugate gradient algorithm (Fig. 3). This optimization was achieved using the Open Babel module of PyRx, and the ligands were subsequently converted into AutoDock-compatible pdbqt format, facilitating the subsequent docking exploration. To facilitate the docking studies, an AutoDock grid box was meticulously positioned around the binding site where the co-crystallized ligand was situated. The subsequent analysis and visualization of the docking results, binding poses, and molecular interactions were conducted using a suite of tools, including BIOVIA Discovery Studio 2021, Molegro Molecular Viewer, and Chimera X [26, 27]. Binding energies and the molecular interaction profiles of the compounds were compared with those of the co-crystallized inhibitory ligands in DNA Gyrase, Lanosterol 14 alpha-demethylase, and KEAP1/NRF2 proteins. A summary of these values is presented in Table 3. The precise binding site positions of FHM with different proteins are also detailed in Table 4.

In compound FHM, we observed notable hydrogen-bond interactions with ARG385, primarily involving the -C=O methanone group that serves as a bridge between the pyrazole and piperidine moieties. At the same time, this residue participated in π-alkyl interactions with the fluorine-substituted phenyl group. ARG469 was found to engage in alkyl interactions with the piperidine ring, while LEU383 exhibited π-alkyl interactions with both the chlorine-substituted aromatic phenyl group and

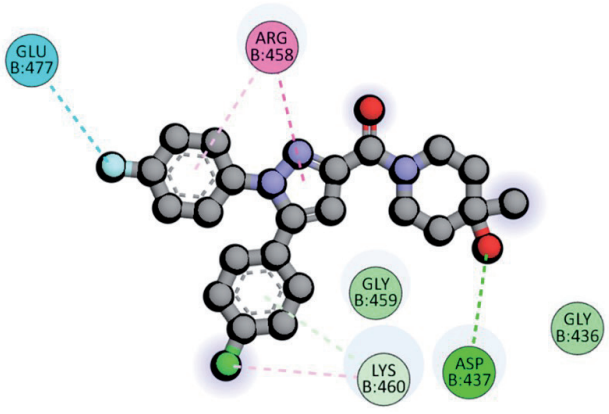

Fig. 3. 2D representation of the binding poses of FMH in the active site of Staphylococcus aureus DNA Gyrase.

Table 4. Molecular interaction summary of the FHM compound with different target proteins.

Target Protein	Binding Energy (Kcal/mol)	Interacting Amino acids	Nature of interaction
DNA Gyrase	-4.5	ASP437, ARG458, GLU477, LYS460, GLY459, GLY436	H-bond, Hydrophobic (p-Alkyl, Amide-p stacked, p-s)
Lanosterol 14 alpha demethylase	-7.4	LEU380, TYR126, ARG385, LEU383, ARG469, HIS468, PHE384, SER382, HIS381, HEM601	Hydrophobic ((p-Alkyl, Alkyl, p-p T-shaped, p-s)
KEAP1-NRF2	-9.3	SER508, ARG483, SER602, ALA556, TYR334, ARG415, ILE461, PHE577, PHE478, TYR525, GLY462, GLY509, ILE416, GLY364, GLY603, ASN382	H-bond, Hydrophobic (Alkyl, p-Alkyl p-s)

the pyrazolo heterocyclic ring. Furthermore, the HEM group displayed relatively weaker, non-classical carbon-hydrogen interactions.

Comparatively, Fluconazole displayed a lower binding energy of -7.8 Kcal/mol when contrasted with the FHM compound. It established a hydrogen bond with TYR140, contributing to its stabilization. Moreover, Fluconazole's stability was further reinforced through diverse interactions, such as pi-sigma interactions with LEU380, π–π stacked interactions, and π–π T-shaped interactions with TYR126 and PHE236 residues, facilitated by the presence of triazole rings. The HEM moiety was involved in a hydrophobic interaction with the difluoro-substituted aromatic ring. Additionally, the triazole and halogen-substituted ring engaged in π–alkyl interactions with ILE139, LEU380, and VAL150 residues, while GLY314 exhibited halogen interactions with the fluorine groups.

FHM had predominantly hydrophobic interactions with the anti-fungal target of Lanosterol 14α demethylase with a binding energy of -7.4 Kcal/mol. LEU380 had π–σ interactions through the pyrazole ring and π–π T-shaped interactions with PHE134, TYR126, and HIS381 residues. The HEM moiety in the active site also had an interaction with the aromatic ring substituted with Bromine. MET509 had π–alkyl interactions with aromatic and heterocyclic rings. The Methyl group substituted on the triazole ring and had alkyl interactions with PHE384 and PHE241 residues, and then it had Vander Waals interactions with the surrounding binding site amino acid residues. Molecular interactions, the binding site, and the binding pose of FHM can be visualized in Fig. 4.

Fluconazole had a better binding energy of -7.8 K.cal/mol compared to FHM, exhibiting an H-bond with TYR140. It is also stabilized with various types of interactions, like π–σ interactions with LEU380, π–π stacked, and π–π T-shaped interactions with TYR126 and PHE236 residues through the triazole rings. Haem moeity also had a hydrohobic interaction with the difluoro substituted aromatic ring, and then the ILE139, LEU380, and VAL150 residues had π–alkyl interactions with the triazole and halogen substituted ring. GLY314 had halogen interactions with the fluorine groups.

FHM also reveals noteworthy interactions, forming three hydrogen bonds with SER602, ARG483, and SER508 residues. One hydrogen bond is established between the methanone linker, connecting the pyrazole

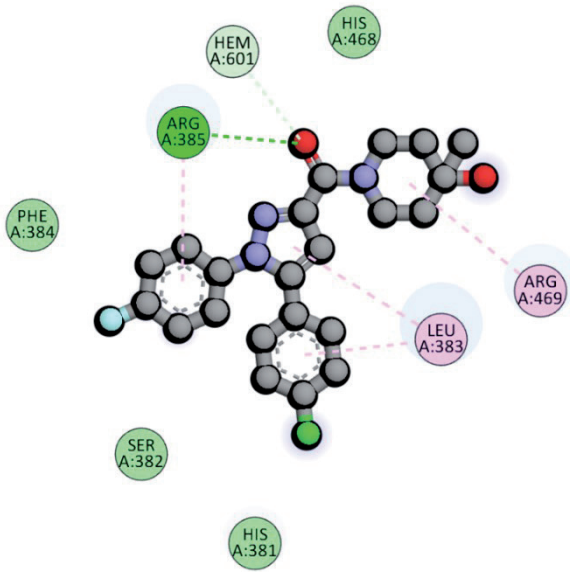

Fig. 4. 2D representation of the binding poses of FMH and in the active site of S. cerevisiae Lanosterol 14α demethylase.

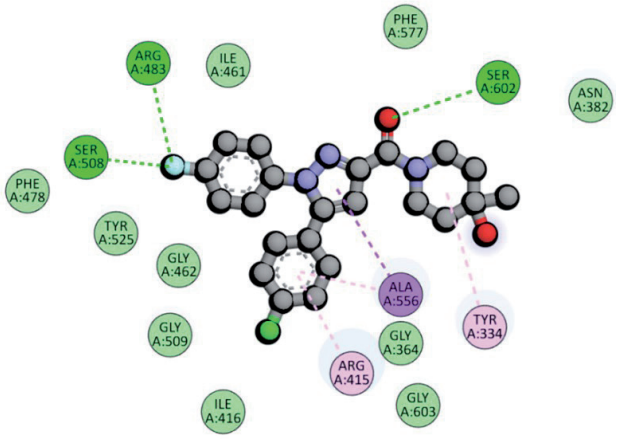

Fig. 5. 2D representation of the binding poses of the FHM molecule and in the active site of the KEAP1-NRF2 protein.

and substituted piperidine, and SER602. The remaining two hydrogen interactions with ARG483 and SER508 are mediated by the halogen (-F) on the phenyl group linked to the pyrazole ring. ALA556 participates in π–sigma interaction with the pyrazole ring and π–alkyl interaction with the chlorine-substituted aromatic phenyl ring. TYR334 contribute to alkyl interactions with the cycloalkyl piperidine group. Interestingly, FHM exhibits a hydrogen bond interaction with SER602. These diverse molecular interactions have the potential to contribute to the activity of these compounds.

Edaravone displays a single H-bond interaction with ALA556 and a π–alkyl interaction with the ARG415 residue. In contrast, J6Q forms two hydrogen bonds with SER602 and SER508 active site residues, involving the nitrogen of the benzotriazole ring and the sidechain propanoic acid, respectively. Remarkably, FHM and J6Q all share a common H-bond interaction with the SER602 residue. The chloro-substituted phenyl ring engages in pi-pi stacked interactions with TYR525, ALA556 participates in π–sigma and π–alkyl interactions with the aromatic ring area of benzotriazole, and TYR572 forms π–alkyl interactions with the chlorine on the phenyl ring. The compounds FHM and J6Q interact with similar critical active site residues such as SER602, TYR525, and ALA556. Fig. 5 provides visual representations of the molecular interactions, binding sites, and orientations of FHM, Edaravone, and J6Q within the protein's active site. Regarding their anti-bacterial and antioxidant targets, FHM demonstrates superior binding energy and interaction profiles compared to the co-crystallized inhibitors. Post-docking analysis establishes a strong correlation between in silico and in vitro results for the FHM compound. This suggests their potential as novel agents in antimicrobial and antioxidant applications. Further exploration, particularly into their antioxidant mechanism via the Keap1-Nrf2 pathway, could position these compounds as promising candidates for the development of innovative lead compounds [28-30].

Conclusions

In this investigation, we have successfully crafted a highly functionalized pyrazole derivative, denoted as FHM, featuring a 4-methylpiperidin-4-ol substitution. FHM's physicochemical attributes have been meticulously scrutinized through ^{1}H-NMR, FT-IR, and LC-MS analyses, offering a comprehensive insight into its properties. Additionally, computational methods have been employed to thoroughly assess FHM's photophysical properties. The optimized molecular geometry and HOMO-LUMO plots were determined using the DFT-B3LYP-6-31G(d) basis set. The calculated global chemical reactivity descriptors, based on HOMO (-5.428 eV) and LUMO (-1.326 eV) values, highlight FHM's notable electrophilic character, suggesting reactivity and relatively lower stability. Moreover, electron-deficient regions identified through DFT analyses suggest potential applications in pharmaceutical design. The in-vitro evaluation of FHM revealed significant antimicrobial, antifungal, and antioxidant activities, underscoring its promising biological applications. In-silico molecular docking studies further indicated FHM's favorable interactions with target receptors, surpassing the medicinal standard drug Rifampicin. The synthesized molecule emerges as a promising candidate in drug design, showcasing potential efficacy in regulating pathogenic behavior. Overall, these findings position FHM as a prospective agent for diverse biological applications.

Acknowledgments

Princess Nourah bint Abdulrahman University Researchers Supporting Project number (PNURSP2024R76), Princess Nourah bint Abdulrahman University, Riyadh, Saudi Arabia.

Conflict of Interest

The authors declare no conflict of interest.

Reference

1. MUSTAFA G., ZIA-UR-REHMAN M., SUMRRA S.H., ASHFAQ M., ZAFAR W., ASHFAQ M. A critical review on recent trends on pharmacological applications of pyrazolone endowed derivatives. Journal of Molecular Structure, **1262**, 133044, **2022**.
2. HOMMA T., KOBAYASHI S., SATO H., FUJII J. Edaravone, a free radical scavenger, protects against ferroptotic cell death in vitro. Experimental Cell Research, **384** (1), 111592, **2019**.
3. DA SILVA T.L., COSTA C.S.D., DA SILVA M.G.C., VIEIRA M.G.A. Overview of non-steroidal anti-inflammatory drugs degradation by advanced oxidation processes. Journal of Cleaner Production, **346** (4), 131226, **2022**.
4. MOULINET, T., MOUSSU A., PIERSON L., PAGLIUCA S. The many facets of immune-mediated thrombocytopenia: Principles of immunobiology and immunotherapy. Blood Reviews, 101141, **2023**.
5. WANG X., DU S., ZHANG R., JIA X., YANG T., ZHANG X. Drug-drug cocrystals: Opportunities and challenges. Asian Journal of Pharmaceutical Science, **16** (3), 307, **2021**.
6. DE PAULA V.V., ARAÚJO-SILVA G., FERNANDES N.S., MOUTA A.N., NUNES T.L., DE PAIVA A.L.C., DE MACÊDO L.B., ARCOVERDE K.N., URIZAR J.T.P. Pharmacokinetic profiles of the two major active metabolites of metamizole, 4-methylaminoantipyrine (MAA) and 4-aminoantipyrine (AA), after intravenous injection in cats. Research in Veterinary Science, **155**, 156, **2023**.
7. ZHANG Y., WANG J., CUI H., GAO S., YE L., LI Z., NIE S., HAN J., WANG A., LIANG B. Environmental occurrence, risk, and removal strategies of pyrazolones:

A critical review. Journal of Hazardous Materials, **460** (9), 132471, **2023**.
8. HIMLY M., JAHN-SCHMID B., PITTERTSCHATSCHER K., BOHLE B., GRUBMAYR K., FERREIRA F., EBNER H., EBNER C. IgE-mediated immediate-type hypersensitivity to the pyrazolone drug propyphenazone. The Journal of Allergy and Clinical Immunology, **111** (4), 882, **2003**.
9. AKOCAK S., LOLAK N., GIOVANNUZZI S., SUPURAN C.T. Potent and selective carbonic anhydrase inhibition activities of pyrazolones bearing benzenesulfonamides. Bioorganic and Medical Chemistry Letters, **95** (8), 129479, **2023**.
10. MEZGEBE K., MULUGETA E. Synthesis and pharmacological activities of azo dye derivatives incorporating heterocyclic scaffolds: a review. RSC Advances, **12** (40), 25932, **2022**.
11. YERBANGA, I.W., DIALLO S.N., ROUAMBA T., RESENDIZ-SHARPE A., LAGROU K., DENIS O., RODRIGUEZ-VILLALOBOS H., MONTESINOS I., BAMBA S. Performances of disk diffusion method for determining triazole susceptibility of *Aspergillus* species: Systematic review. Journal of Medical Mycology, **33** (4), 101413, **2023**.
12. GOTO R., JIN W., WACHINO J.I., ARAKAWA Y., KIMURA K. Improved disk diffusion method for simple detection of group B streptococci with reduced penicillin susceptibility (PRGBS). Diagnostic Microbiology and Infectious Disease, **105** (3), 115881, **2023**.
13. LOHIT N., MARIDEVARMATH C.V., KHAZI I.A.M., MALIMATH G.H. Photophysical and computational studies on optoelectronically active thiophene substituted 1,3,4- oxadiazole derivatives. Journal of Photochemistry and Photobiology A Chemistry, **368**, 200, **2019**.
14. WALKI S., MALIMATH G.H., MAHADEVAN K.M., NAIK S., SUTAR S.M., SAVANUR H., NAIK L. Synthesis, spectroscopic properties, and DFT correlative studies of 3, 3′-carbonyl biscoumarin derivatives. Journal of Molecular Structure, **1243**, 130781, **2021**.
15. PRABHALA P., SUTAR S.M., MANJUNATHA M.R., PAWASHE G.M., GUPTA V.K., NAIK L., KALKHAMBKAR R.G. Synthesis, in vitro and theoretical studies on newly synthesized deep blue emitting 4-(p-methylphenylsulfonyl-5-aryl/alkyl) oxazole analogues for biological and optoelectronic applications. Journal of Molecular Liquids, **360**, 119520, **2022**.
16. NAIK L., THIPPESWAMY M.S., PRAVEENKUMAR V., MALIMATH G.H., RAMESH D., SUTAR S., BUBBLY S.G. Solute-solvent interaction and DFT studies on bromonaphthofuran 1, 3, 4-oxadiazole fluorophores for optoelectronic applications. Journal of Molecular Graphics & Modelling, **118**, 108367, **2023**.
17. PARR R.G., YANG W. Density Functional Theory of Atoms and Molecules, Oxford University Press, New York, **1989**.
18. CHOUDHARY V.K., BHATT A.K., DASH D., SHARMA N. DFT calculations on molecular structures, HOMO–LUMO study, reactivity descriptors and spectral analyses of newly synthesized diorganotin (IV) 2-chloridophenylacetohydroxamate complexes. Journal of the Computational Chemistry, **40** (27), 2354, **2019**.
19. PROFT F.D., GEERLINGS P., HEIDAR-ZADEH F., AYERS P.W. Conceptual Density Functional Theory. Comprehensive Computational Chemistry, **2**, 306, **2024**.
20. REDDY G.M., CAMILO A. Biologically active dihydropyridines: an efficient green synthesis, antimicrobial properties, machine aided results and SARs. Sustainably Chemistry and Pharmacy, **17**, 100303, **2020**.
21. FAHIM A.M., TOLAN H.E., EL-SAYED W.A. Synthesis of novel 1, 2, 3-triazole based Acridine and benzothiazole scaffold N-glycosides with anti-proliferative activity, docking studies, and comparative computational studies. Journal of Molecular Structure, **1251**, 131941, **2022**.
22. EL-BINDARY M.A., EL-BINDARY A.A. Synthesis, characterization, DNA binding, and biological action of dimedone arylhydrazone chelates. Applied Organometallic Chemistry, **36** (4), e6576, **2022.**
23. EL-SONBATI A.Z., DIAB, M.A., EL-BINDARY A.A., NOZHA S.G. Structural and characterization of novel copper (II) azodye complexes. Spectrochimica Acta Part A: Molecular and Biomolecular Spectroscopy, **83** (1), 490-498, **2011.**
24. EL-ZAHED M.M., DIAB M.A., EL-SONBATI A.Z., SAAD M.H., ELDESOKY A.M., EL-BINDARY M.A. Synthesis, spectroscopic characterization studies of chelating complexes and their applications as antimicrobial agents, DNA binding, molecular docking, and electrochemical studies. Applied Organometallic Chemistry, **2023**.
25. SARGIS D., ARTHUR J.O. Small-molecule library screening by docking with PyRx, Methods in molecular biology (Clifton, N.J.), **1263**, 243, **2015**.
26. BAX B.D., CHAN P.F., EGGLESTON D.S., FOSBERRY A., GENTRY, D.R., GORREC F., GIORDANO I., HANN M.M., HENNESSY A., HIBBS M., HUANG J., JONES E., JONES J., BROWN K.K., LEWIS C.J., MAY E.W., SAUNDERS M.R., SINGH O., SPITZFADEN C., SHEN C., SHILLINGS A., THEOBALD A.F., WOHLKONIG A., PEARSON N.D., GWYNN M.N. Type IIA topoisomerase inhibition by a new class of antibacterial agents. Nature, **466**, 935, **2010**.
27. SAGATOVA A.A., KENIYA M.V., WILSON R.K., MONK B.C., TYNDALL J.D. Structural Insights into Binding of the Antifungal Drug Fluconazole to Saccharomyces cerevisiae Lanosterol 14 alpha-Demethylase. Antimicrobial Agents and Chemotherapy, **59**, 4982, **2015**.
28. HEIGHTMAN T.D., CALLAHAN J.F., CHIARPARIN E., COYLE J.E., GRIFFITHS-JONES C., LAKDAWALA A.S., MCMENAMIN R., MORTENSON P.N., NORTON D., PEAKMAN T.M., RICH S.J., RICHARDSON C., RUMSEY W.L., SANCHEZ Y., SAXTY G., WILLEMS H.M.G., WOLFE L., WOOLFORD A.J., WU Z., YAN H., KERNS J.K. Structure-Activity and Structure-Conformation Relationships of Aryl Propionic Acid Inhibitors of the Kelch-like ECH-Associated Protein 1/ Nuclear Factor Erythroid 2-Related Factor 2 (KEAP1/ NRF2) Protein-Protein Interaction. Journal of Medicinal Chemistry, **62** (9), 4683, **2019**.
29. LIMENG S., YUN B., YING S., LIBO W., LIYAO A., QINYING Y. Nrf2 mediates the protective effect of edaravone after chlorpyrifos-induced nervous system toxicity. Environmental Toxicology, **34** (5), 626, **2019**.
30. DAINA A., MICHIELIN O., ZOETE V. Swiss ADME: a free web tool to evaluate pharmacokinetics, druglikeness and medicinal chemistry friendliness of small molecules. Scientific Reports, **7**, 42717, **2017**.